Available online at www.sciencedirect.com
SCIENCE DIRECT®
Tetrahedron: Asymmetry
Tetrahedron: *Asymmetry* 17 (2006) 1049–1055

Interaction of chiral bis-distamycin derivatives with DNAs: electronic circular dichroism study

Lukáš Palivec,[a] Martin Valík,[a] Vladimír Král[a] and Marie Urbanová[b,*]

[a]*Department of Analytical Chemistry, Institute of Chemical Technology, Prague, Technická 5, 166 28 Prague 6, Czech Republic*
[b]*Department of Physics and Measurements, Institute of Chemical Technology, Prague, Technická 5, 166 28 Prague 6, Czech Republic*

Received 1 July 2005; revised 31 March 2006; accepted 3 April 2006
Available online 6 May 2006

Abstract—The new diastereomeric complexes of two oligo-*N*-methylpyrrole peptides, linked by a methano[1,5]-diazocin scaffold with DNA, were prepared. The specificity of the binding modes of (4*S*,9*S*)- and (4*R*,9*R*)-bis-distamycins derivative with ct-DNA explains the observed optical activity of the racemic mixture of distamycin if DNA is present. The bis-distamycin derivative possesses a clear sequence selectivity for A-T rich sequences of DNA, although a nonspecific binding mode with low affinity was also seen for G-C rich sequences. The reversibility of ECD spectra at 5 °C after heating to 90 °C was established.

1. Introduction

The development of short oligopeptides that bind to DNA and have potential applications in targeting tumor growth and antiviral activities has been a goal for more than 30 years.[1,2] One of the most studied oligopeptides is naturally occurring distamycin A[3] and its derivatives. Distamycin A contains three *N*-methylpyrrole carboxamide units in a crescent-shaped formation. This shape copies the curvature of the DNA double helix and allows noncovalent interactions such hydrogen-bonding, hydrophobic, van der Waals, and electrostatic binding modes of distamycin A with DNA. The mechanism of the interaction was studied by various techniques, for example, NMR,[4,5] footprinting,[4,6–8] X-ray,[9] electronic circular dichroism (ECD)[4,10–14] and by ab initio modeling.[15] It was found that distamycin A and its derivatives bind to the minor groove of DNA rich in A-T sequences. Moreover, increasing the number of pyrrole units of the distamycin A analogues led to an increase in the sequence selectivity for A-T rich fragments of DNA.[12] In addition, modification of distamycin analogues, such as replacing *N*-methylpyrrole by *N*-methylimidazole ring, can cause a change of selectivity from A-T to G-C base pairs.[13] One of the most interesting findings on the binding mechanism was that distamycin analogues can bind to DNA as monomers, as well as antiparallel dimers.[11,14] Based on these observations, several bis-distamycin derivatives with various linkers have been prepared to increase the affinity and specificity of the interaction with DNA. It was found that conformationally constrained linkers are more effective for binding to DNA than flexible polymethylene linking chains, and that the stereochemistry of the linkers can control the binding.[3]

Herein, we report bis-distamycin derivatives **1**–**4** (Scheme 1) composed of two *N*-methylpyrrole carboxamide tails containing various numbers of *N*-methylpyrrole units at both sides[16] linked by a Tröger's base (TB) scaffold. The

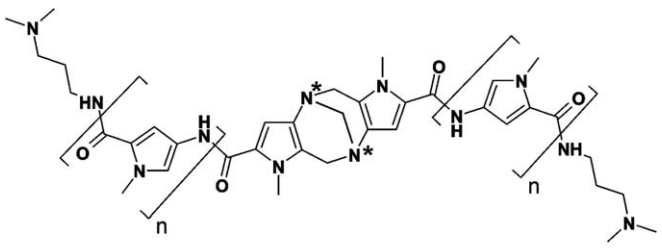

1 n=0
2 n=1
3 n=2
4 n=3

Scheme 1.

* Corresponding author. Tel.: +420 220443036; fax: +420 220444334; e-mail: marie.urbanova@vscht.cz

0957-4166/$ - see front matter © 2006 Elsevier Ltd. All rights reserved.
doi:10.1016/j.tetasy.2006.04.001

TB motive is attractive in the molecular design of receptors due to its rigid V-shape, which copies the geometry of the DNA minor groove.[17–19] In addition, the geometry of TB has been used in the preparation of various receptor systems, as well as DNA active compounds that bind DNA with high sequence selectivity and enantioselectivity.[20–22] This paper also describes a spectroscopic study of the interaction between novel racemic Tröger's base bis-distamycin (TB-dist) analogues **1**–**4** and DNAs, including ct-DNA, $(dA\text{-}dT)_{10}$ and $(dG\text{-}dC)_{10}$. The stereoselectivity influence of TB spacer on binding of TB-dist was studied on chiral (4*S*,9*S*)-**4** and (4*R*,9*R*)-**4**.

2. Results and discussion

2.1. Interaction of racemic TB-dist 1–4 with ct-DNA

Figure 1 shows the absorption spectra of the free racemic distamycin derivatives, free ct-DNA, and their complexes with ct-DNA measured in NaCl/cacodylate buffer. Pure TB-dist **1**–**4** show the characteristic absorption bands at 242 nm, as well as the second absorption maximum observed at 288, 306, 311, and 314 nm for **1**, **2**, **3**, and **4**, respectively (Fig. 1A). Figure 1B shows the absorption spectra of free ct-DNA and ct-DNA/TB-dist complexes. The absorption band of free ct-DNA with the maximum at 257 nm (dashed lines) overlaps the TB-dist band at 242 nm. The absorption above 300 nm obviously corresponds to the TB-dist part of complexes. This signal is red shifted compared to free TB-dist and is manifested as the resolved maximum at 308, 314, and 320 nm for **2**, **3**, and **4** (solid lines), respectively. In the ct-DNA/**1** complex, the TB-dist part of the complex is manifested as a shoulder at 270 nm. The red shifts, except of **1**, and the significant decrease of intensity in UV absorption spectra of TB-dist observed after addition of ct-DNA prove the interaction between both partners.[23–25]

Figure 2 shows the ECD spectra of TB-dist **1**–**4** in the presence of ct-DNA, and TB-dist **4** in the presence of $(dA\text{-}dT)_{10}$ and $(dG\text{-}dC)_{10}$, together with the spectra of free DNAs. All samples exhibit the ECD pattern below the 300 nm with

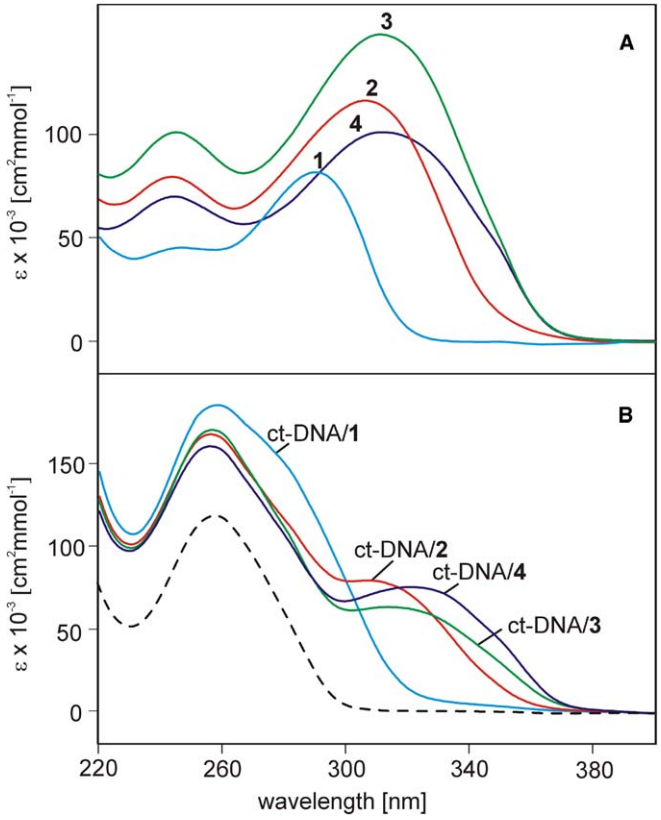

Figure 1. UV–vis absorption spectra of (A) pure TB-dist **1**–**4**, (B) ct-DNA/**1**–**4** complexes (—), and pure ct-DNA (---), c(TB-dist) = 0.2 mM, c(DNA) = 1.6 mM in cacodylate buffer (0.02 M) with NaCl (0.1 M).

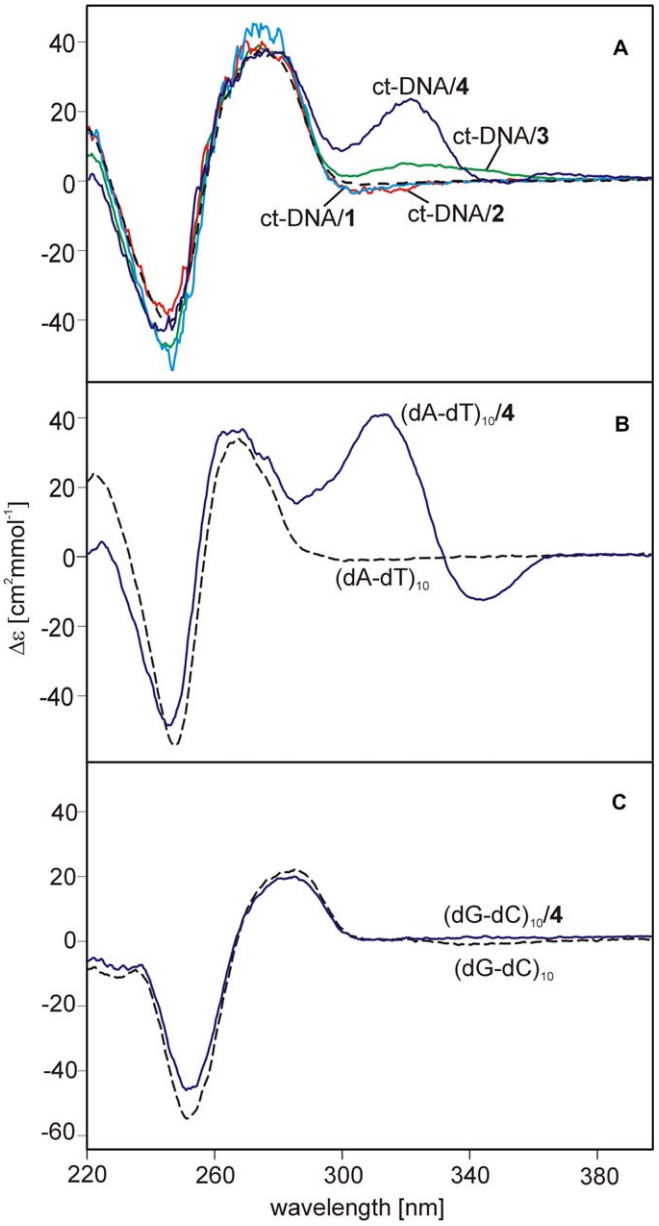

Figure 2. ECD spectra of complexes (—) (A) ct-DNA/**1**–**4**; (B) $(dA\text{-}dT)_{10}$/**4**; (C) $(dG\text{-}dC)_{10}$/**4**, and free DNAs (---) (A) ct-DNA, (B) $(dA\text{-}dT)_{10}$, (C) $(dG\text{-}dC)_{10}$. Concentration is the same as in Figure 1.

positive and negative maxima typical of DNA. Neither the free DNAs nor the free TB-dist racemates exhibit ECD signals above 300 nm. Well resolved ECD signals in the 300–400 nm spectral region were observed for complexes ct-DNA/**3** and ct-DNA/**4** (Fig. 2A). TB-dist **3** gives a positive ECD band at 320 nm, while TB-dist **4** gives the positive ECD band more than three times larger with the maximum at 323 nm, together with the weak negative band at 353 nm. These ECD bands were not observed for the ct-DNA/**1** complex as well as for the ct-DNA/**2** complex. These results are consistent with previous observations[12] that the intensity of the ECD pattern increases with the number of pyrrole units in distamycin derivative. In addition, the spatial arrangement of *N*-methylpyrrole-TB core partially restricts the interaction of the TB-dist **1** and **2** short tails with DNA bases. Therefore, the specificity of minor groove binding of ct-DNA cannot be fully utilized. In this case, the TB-dist molecules can possess several non-specific binding modes in the complex with ct-DNA, and the induction of ECD signal does not occur. On the other hand, the geometry of **3** and especially **4** is more suitable for the recognition by ct-DNA and the characteristic ECD pattern appears. Based on these results, we will discuss only the TB-dist **4** and its interaction with DNAs in the following study.

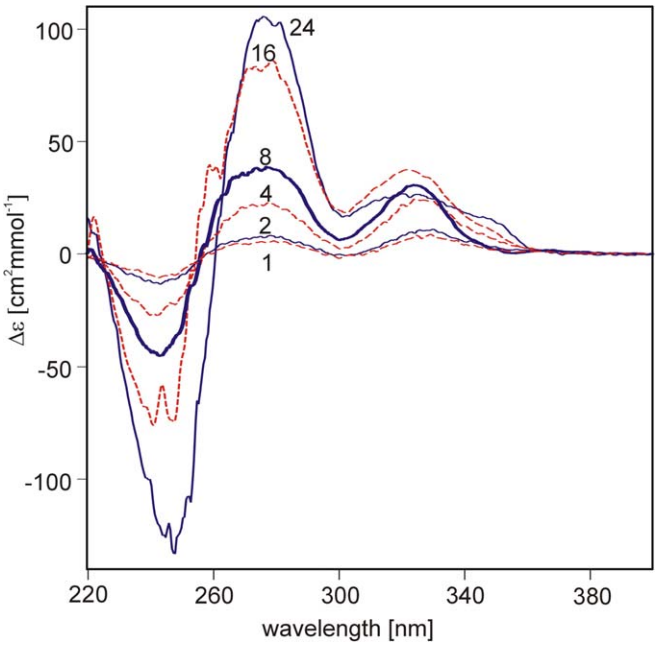

Figure 3. ECD spectra of ct-DNA/**4** complexes for different ratios R (denoted by numbers at the spectra). c(TB-dist) = 0.2 mM.

The sequence selectivity of the binding of **4** to DNA was examined using sequential oligonucleotides $(dA\text{-}dT)_{10}$ and $(dG\text{-}dC)_{10}$. Above 300 nm, the ECD signal shape of **4** in the presence of $(dA\text{-}dT)_{10}$ is very similar to the spectrum observed in the presence of ct-DNA (cf. Fig. 2B and A) but is about twice as great when compared to ct-DNA/**4**, which is in agreement with approximately 50% amount of A-T base pairs contained in natural DNA. No ECD of **4** in the presence of $(dG\text{-}dC)_{10}$ was observed above 300 nm (Fig. 2C). In agreement with previous studies of distamycin and its derivatives,[3,11,14] the selectivity of TB-dist **4** to A-T rich sequences of DNA was confirmed.

Figure 3 shows the dependence of the ECD spectra on the molar ratio $R = [DNA]_{bp}/[TB\text{-}dist]$, where $[DNA]_{bp}$ is the concentration of ct-DNA base pairs and [TB-dist] is the concentration of distamycin derivatives. The sample for $R = 8$ possesses the highest relative signal of the distamycin part of complex comparing to the DNA part of complex without their substantial overlap, and enables the simultaneous spectroscopic study of both parts of the complex. Therefore, the value of $R = 8$ was chosen in this study.

Figure 4A shows the temperature dependent ECD spectra of ct-DNA/**4** complex for selected temperatures obtained by the sample warming from 20 to 90 °C and then cooling down to 20 °C. The intensities of positive and negative bands of the TB-dist **4** part of the ct-DNA/**4** complex for all measured temperatures are displayed in the column graph in Figure 4B. The negative ECD band of **4** increases its intensity with increasing temperature, while the intensity of the positive one remains almost unchanged. Above 70 °C, both the positive and negative bands start decreasing in intensity and at 90 °C they almost disappear. Moreover, at 90 °C a significant decrease of ECD signal at 246 and 274 nm typical for DNA was observed. We interpret the increase of the negative band while the temperature is increased up to 70 °C as the consequence of 'breathing' of the DNA chain which becomes more outstretched. Therefore, **4** can reach the appropriate orientation in minor groove more easily. At 90 °C, the melting of DNA duplex occurs, which results in a decrease of the observed ECD bands at 246 and 274 nm typical for DNA. Subsequently, the ct-DNA/**4** complex collapses which causes substantial decrease of both positive and negative bands typical for the TB-dist **4** part of complex. Slow cooling to 20 °C leads to a reversal of the original intensity of the positive as well as negative band, to values observed before heating of the sample. Besides these changes in the ECD magnitude, the blue shift of the negative band from 352 to 343 nm and positive band from 323 to 314 nm occurs. It follows from these observations that after slow cooling back to 20 °C, when the denaturated duplex is folded back, the complex with **4** is formed again.

To elucidate the observations of racemic **4** demonstrated in Figures 1–5, the ECD study of enantiomers of TB-dist **4** and their interactions with ct-DNA, $(dA\text{-}dT)_{10}$, and $(dG\text{-}dC)_{10}$ was carried out.

2.2. Enantiomerically pure (4*S*,9*S*)-4 and (4*R*,9*R*)-4, and their interaction with DNAs

The ECD spectra of the free enantiomers (4*S*,9*S*)-**4** and (4*R*,9*R*)-**4** and in the presence of ct-DNA, $(dA\text{-}dT)_{10}$ and $(dG\text{-}dC)_{10}$ are shown in Figure 5. Enantiomer (4*R*,9*R*)-**4** provides two positive signals with maxima at 250 and 305 nm and a strong negative signal at 337 nm (Fig. 5A, (—)); enantiomer (4*S*,9*S*)-**4** provides the spectrum with opposite sign (Fig. 5A, (---)). In the presence of ct-DNA, the ECD pattern of both enantiomers shows the red shift

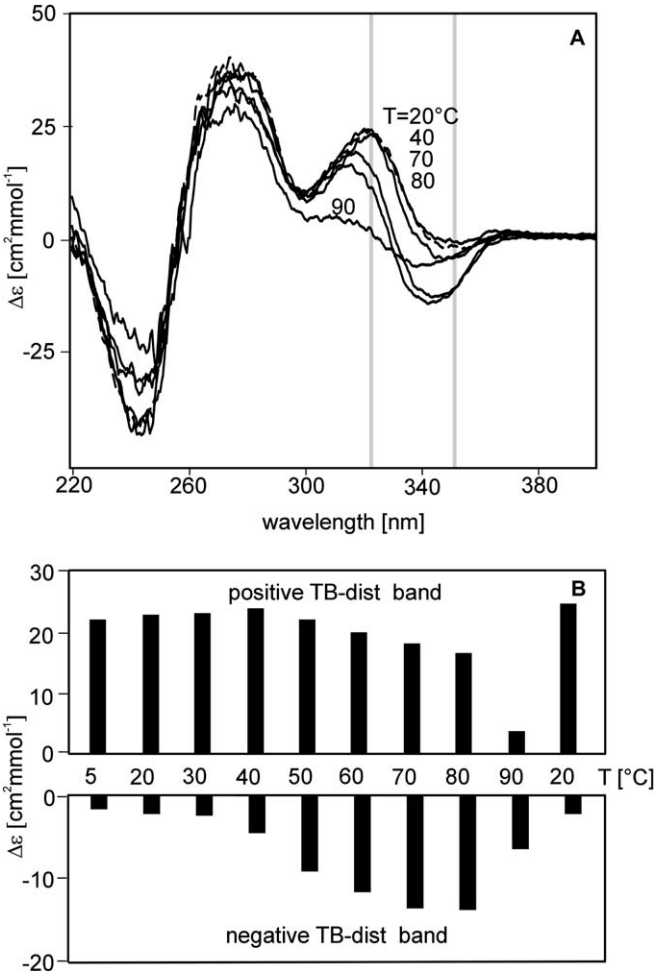

Figure 4. (A) Temperature dependent ECD spectra of ct-DNA/**4** complex during the heating (—), and after cooling to 20 °C (---), (B) temperature dependence of the ECD band intensity of TB-dist part of ct-DNA/**4** complex (B). Concentration is the same as in Figure 1.

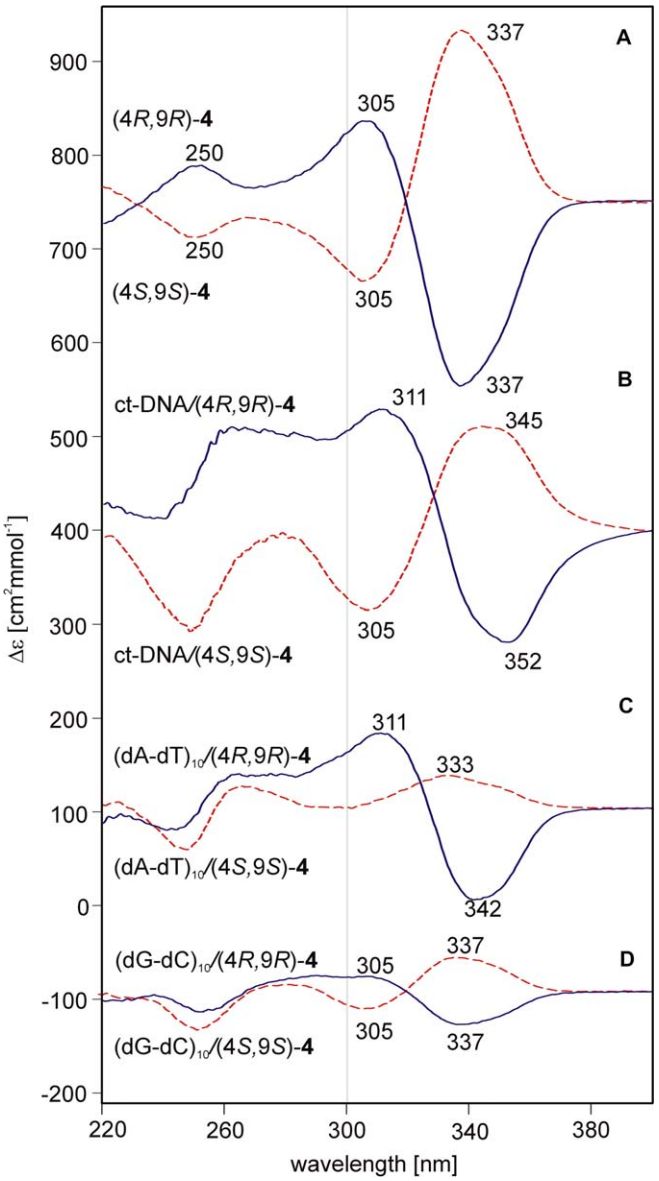

Figure 5. ECD spectra of (A) pure enantiomers (4*R*,9*R*)-**4** (—) and (4*S*,9*S*)-**4** (---), and their complexes with (B) ct-DNA, (C) $(dA\text{-}dT)_{10}$, (D) $(dG\text{-}dC)_{10}$. Concentration is same as in Figure 1.

and a significant intensity decrease in the region 300–400 nm, indicating the interaction of both enantiomers with ct-DNA (Fig. 5B). Below 300 nm, the ECD signal of both enantiomers of **4** is overlapped by ct-DNA bands. The variation of the ECD signals originating in the interaction of **4** with ct-DNA is markedly different for both enantiomers. The complex of ct-DNA/(4*R*,9*R*)-**4** (Fig. 5B, (—)) shows the shifts of both CD bands 305→311 nm and 337→352 nm, while the complex of ct-DNA/(4*S*,9*S*)-**4** (Fig. 5B, (---)) exhibits only shift of positive signal 337→345 nm. Similar results were obtained for (4*S*,9*S*)-**4** and (4*R*,9*R*)-**4** with $(dA\text{-}dT)_{10}$ (Fig. 5C). The complex $(dA\text{-}dT)_{10}$/(4*R*,9*R*)-**4** shows the red shift of the positive band 305→311 and negative band 337→342 nm, and the decrease of the ECD intensity of both bands (Fig. 5C, (—)). The complex $(dA\text{-}dT)_{10}$/(4*S*,9*S*)-**4** provides a blue shift of positive band 337→333 nm and distinctive intensity decrease, while the negative band originally at 305 nm almost disappears (Fig. 5C, (---)). Figure 5D shows the ECD of both enantiomers in the presence of $(dG\text{-}dC)_{10}$. For the $(dG\text{-}dC)_{10}$/(4*R*,9*R*)-**4** complex, the positions of the positive and negative bands at 305 and 337 nm, respectively, are identical with the free (4*R*,9*R*)-**4** enantiomer (Fig. 5D, (—)), although the intensity of both bands is significantly decreased. Complex $(dG\text{-}dC)_{10}$/(4*S*,9*S*)-**4** gives the ECD pattern of the same shape as $(dG\text{-}dC)_{10}$/(4*R*,9*R*)-**4**, but with an opposite sign (Fig. 5D, (---)). The ECD differences between the complexes of two chiral partners—DNAs and enantiomer (4*R*,9*R*)-**4** or (4*S*,9*S*)-**4**—can be explained as a consequence of the formation of complexes analogous to diastereomers, molecules with two or more chiral centers, which possess nonmirror-symmetrical ECD spectra. A similar phenomenon was observed previously on iron(II) mixed–ligand complexes with DNA[26] as well as on complexation of bilirubin with small chiral molecules.[27,28] The effect was described as the equilibrium displacement in favor of either enantiomer upon addition of optically active substances.

2.3. Comparison between ECD spectra of racemic 4 and its enantiomers (4*S*,9*S*)-4 and (4*R*,9*R*)-4

It is obvious from Figures 2–4 that racemic **4** in the presence of ct-DNA provides the ECD pattern in 300–400 nm spectral region, although racemic **4** itself does not exhibit ECD in agreement with observed mirror image spectra of individual enantiomers presented in Figure 5A. It is also evident from Figure 5 that (4*R*,9*R*)-**4** and (4*S*,9*S*)-**4** enantiomers form diastereomeric complexes with ct-DNA, as well as $(dA\text{-}dT)_{10}$, which possess different ECD spectra for each enantiomer. In Figure 6, the ECD spectra of racemic **4** with ct-DNA, $(dA\text{-}dT)_{10}$, and $(dG\text{-}dC)_{10}$ are compared to the calculated spectra obtained as a superposition of the experimental spectra of both (4*R*,9*R*)-**4** and (4*S*,9*S*)-**4** diastereomeric complexes with DNAs. It is obvious that the experimental and calculated spectra possess closely similar spectral patterns. Therefore, the experimental spectra of racemic **4** with DNA are interpreted as the superposition of the ECD spectra of the diastereomeric complexes (4*R*,9*R*)-**4** and (4*S*,9*S*)-**4** with DNA. It was expected that both enantiomers in the racemic mixture would interact with all DNAs and form diastereomeric complexes. The same is valid for the oligonucleotide $(dA\text{-}dT)_{10}$ (Fig. 6B): The ECD signal of complex $(dA\text{-}dT)_{10}$/**4** above 300 nm arises from the superposition of individual nonmirror-symmetrical ECD spectra of $(dA\text{-}dT)_{10}$/(4*R*,9*R*)-**4** and $(dA\text{-}dT)_{10}$/(4*S*,9*S*)-**4** diastereomeric (cf. Figs. 5C and 6B). On the other hand, the absence of this ECD signal above 300 nm of $(dG\text{-}dC)_{10}$/**4** complex (Fig. 6C) is a consequence of the superposition of the individual mirror symmetrical ECD spectra of $(dG\text{-}dC)_{10}$/(4*R*,9*R*)-**4** and $(dG\text{-}dC)_{10}$/(4*S*,9*S*)-**4** diastereomeric complexes (cf. Figs. 5D and 6C). Based on these results, it is obvious that the shape and intensity of ECD observed for ct-DNA/**4** complex is given by the formation of diastereomeric complexes of **4** with both A-T and G-C base pairs. The complexation of racemic **4** with A-T base pairs provides diastereomeric complexes possessing different ECD's, which is probably the consequence of specific binding mode between two chiral partners—helical duplex and individual enantiomers. The specificity of binding mode between **4** and G-C base pairs is probably poor and, therefore, the chirality of **4** does not play a significant role and the ECD spectra of both diastereomeric complexes are the same except for the sign. It is also evident that the experimental spectrum intensity of DNA/**4** above 300 nm (Fig. 6A) reaches only 50% of the experimental spectrum intensity of $(dA\text{-}dT)_{10}$/**4** (Fig. 6B), which is in coincidence with 50% amount of A-T base pairs in ct-DNA. Considering the facts mentioned above, the ECD spectrum above 300 nm of ct-DNA/**4** complex is given by the contribution of specific binding mode of **4** with A-T base pairs, while the contribution of binding with G-C base pairs is negligible.

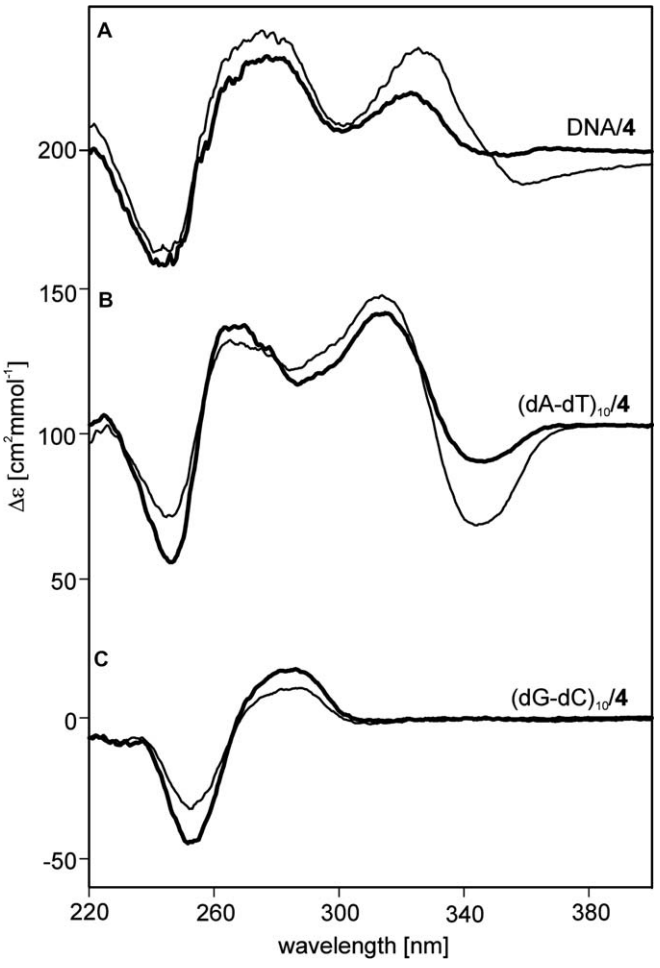

Figure 6. The comparison of the experimental ECD of **4** (thick lines) and the superposition of experimental ECD spectra of (4*R*,9*R*)-**4** and (4*S*,9*S*)-**4** (thin lines) measured in the presence of (A) ct-DNA, (B) $(dA\text{-}dT)_{10}$, (C) $(dG\text{-}dC)_{10}$.

3. Conclusions

The UV–vis absorption spectra of ct-DNA complexes with **2**–**4** confirm the interaction between both partners. For TB-dist **1** in the presence of ct-DNA, no clear proof of interaction was observed. Significant ECD signal of **3** and **4** in the presence of ct-DNA indicates the specific minor groove binding mode of both TB-dist with ct-DNA. We assume that the binding specificity of TB-dist **3** and mainly TB-dist **4** arises from a proper arrangement of TB-dist in complex with ct-DNA. Derivative **2** shows no characteristic ECD signal in the presence of ct-DNA, therefore, the specificity of binding mode is probably suppressed. The length of the *N*-methylpyrrole tails of the novel bis-distamycin derivatives **1**–**4** linked by Tröger's base scaffold significantly influences the specificity of the interaction with ct-DNA. The sequence selectivity of TB-dist **4** was determined using the synthetic oligonucleotides $(dA\text{-}dT)_{10}$ and $(dG\text{-}dC)_{10}$. The similarity between the ECD bands of the $(dA\text{-}dT)_{10}$/**4** and ct-DNA/**4** complexes and absence of the band characteristic for the distamycin derivatives in the $(dG\text{-}dC)_{10}$/**4** complex demonstrates the selectivity of **4** for the A-T rich sequences. For elucidation of interaction between racemic **4** and DNAs, the study of (4*R*,9*R*)-**14** and (4*S*,9*S*)-**14** with DNAs was carried out.

The binding mode between **4** and ct-DNA is influenced by the geometry of **4**; it also depends on the structure of

ct-DNA. The B-form of ct-DNA is influenced by the temperature as well as ionic strength. On increasing the temperature below the melting point, the ct-DNA duplex becomes more outstretched and the minor groove is more accessible for binding of **4**. On the other hand, the width of the minor groove at higher ionic strength is smaller; therefore, the interaction with **4** is restricted. However, the effect of ionic strength on the better solubility of ct-DNA and TB-dist **4** is important.

It was shown that the originally opposite sign and symmetrical ECD spectra of the enantiomers (4*R*,9*R*)-**4** and (4*S*,9*S*)-**4** exhibit significant difference above 300 nm in the presence of ct-DNA as well as $(dA\text{-}dT)_{10}$. This fact can be explained by the formation of diastereomeric complexes DNAs/(4*R*,9*R*)-**4** and DNAs/(4*S*,9*S*)-**4**, which possess different chiroptical properties. The difference between the ECD spectra of both diastereomeric complexes is caused by specificity and the affinity of the binding mode between two chiral partners—helical duplex and both enantiomers. The complexes of enantiomers (4*R*,9*R*)-**4** and (4*S*,9*S*)-**4** with $(dG\text{-}dC)_{10}$ possess opposite signs and symmetric ECD spectra above 300 nm. This is probably the consequence of a nonspecific binding mode with low affinity between $(dG\text{-}dC)_{10}$ and both (4*R*,9*R*)-**4** and (4*S*,9*S*)-**4**. However, both enantiomers of racemic **4** participate in interaction with all DNAs. This conclusion is obvious from the similarity between ECD spectra of DNAs complexes with racemic **4** and with superpositions of (4*R*,9*R*)-**4** and (4*S*,9*S*)-**4**.

4. Experimental

Calf thymus DNA sodium salt and sodium cacodylate trihydrate were purchased from Sigma–Aldrich, while $(dA\text{-}dT)_{10}$ and $(dG\text{-}dC)_{10}$ were purchased from Generi Biotech, Czech Republic. TB-dist **1**–**4** were prepared in the Department of Analytical Chemistry, Institute of Chemical Technology.[16] For spectroscopic measurements, the reagents were used without further purification.

For UV–vis and ECD measurements, double distilled water with 0.02 M sodium cacodylate trihydrate buffer of pH = 7.4, together with 0.1 M NaCl was used. The solubility of TB-dist in aqueous solvents decreases with an increasing number of *N*-methylpyrrole units. Therefore, in cases of **3** and **4**, the samples were treated in an ultrasonic bath at 70 °C for at least 2 h, until the solution was homogenous. The concentration of **1**–**4** was 0.2 mM and was kept constant, while the concentration of ct-DNA was given by ratio $R = [DNA]_{bp}/[TB\text{-}dist]$ where $[DNA]_{bp}$ is the concentration of ct-DNA base pairs and [TB-dist] is the concentration of distamycin derivatives. Except when studying different ratios *R* (see Fig. 3), all other measurements were carried out at $R = 8$. This value enabled us to simultaneously observe the ECD signals of both ct-DNA and TB-dist **4** without their substantial overlap. DNA/TB-dist complexes were prepared by dissolution of solid amount of ct-DNA in appropriate volume of the TB-dist aqueous solution. The desired homogeneity was obtained when the sample was heated to 70 °C for 1 h, and then slowly cooled down to room temperature and stirred vigorously.

The UV–vis absorption measurement was carried out on a CARY 400 spectrophotometer with a spectral resolution of 1 nm and scanning speed of 600 nm/min. The ECD measurement was carried out on Jasco J-810 spectrophotometer with a spectral resolution of 1 nm, the integration time 1 s for each spectral point, and scanning speed 100 nm/min. Presented spectra are averages of three accumulations. Peltier temperature controller was used for the measurement of temperature dependence ECD spectra. Silica quartz cell of 0.1 cm pathlength was used for both UV–vis and ECD measurements.

Acknowledgements

This work was supported by grant MSM 6046137307 from the Ministry of Education, Youth and Sports of the Czech Republic. We would like to thank Jakub Nový, for stimulating discussions.

References

1. Lown, J. W.; Krowicki, K.; Balzarini, J.; De Clercq, E. *J. Med. Chem.* **1986**, *29*, 1210–1214.
2. Yang, X. L.; Wang, A. H. J. *Pharmacol. Therapeut.* **1999**, *83*, 181–215.
3. Murakami, Y.; Atwood, J. L.; Davies, J. E.; MacNicol, D. D.; Vögtle, F.; Lehn, J.-M. *Comprehensive Supramolecular Chemistry*; Pergamon Press: Oxford, 1996; pp 81–86.
4. Lee, M.; Rhodes, A. L.; Wyatt, M. D.; Forrow, S.; Hartley, J. A. *Biochemistry* **1993**, *32*, 4237–4245.
5. Singh, M. P.; Plouvier, B.; Hill, G. C.; Gueck, J.; Pon, R. T.; Lown, J. W. *J. Am. Chem. Soc.* **1994**, *116*, 7006–7020.
6. Baker, B. F.; Dervan, P. B. *J. Am. Chem. Soc.* **1989**, *111*, 2700–2712.
7. Griffin, J. H.; Dervan, P. B. *J. Am. Chem. Soc.* **1986**, *108*, 5008–5009.
8. Kwok, Y.; Zhang, W.; Schroth, G. P.; Liang, C. H.; Alexi, N.; Bruice, T. W. *Biochemistry* **2001**, *40*, 12628–12638.
9. Han, G. W.; Kopka, M. L.; Cascio, D.; Grzeskowiak, K.; Dickerson, R. E. *J. Mol. Biol.* **1997**, *269*, 811–826.
10. Blanco, J. B.; Vázquez, M. E.; Martinez-Costas, J.; Castedo, L.; Mascarenas, J. L. *Chem. Biol.* **2003**, *10*, 713–722.
11. Chen, F. M.; Sha, F. *Biochemistry* **1998**, *37*, 11143–11151.
12. Du, W.; Wang, B.; Li, Z.; Xiao, J.; Yuan, G.; Huang, W. *Thermochim. Acta* **2002**, *395*, 257–263.
13. Wyatt, M. D.; Garbiras, B. J.; Lee, M.; Forrow, S. M.; Hartley, J. A. *Bioorg. Med. Chem. Lett.* **1994**, *4*, 801–806.
14. Zhang, W.; Dai, Y.; Schmitz, U.; Bruice, T. W. *FEBS Lett.* **2001**, *509*, 85–89.
15. Bouř, P.; Král, V. *Collect. Czech Chem. Commun.* **2000**, *65*, 631–643.
16. Valík, M.; Malina, J.; Palivec, L.; Foltýno vá, J.; Tkadlecová, M.; Urbanová, M.; Brabec, V.; Král, V. *Tetrahedron* **2006**, in press.
17. Valík, M.; Dolenský, B.; Petříčková, H.; Vašek, P.; Král, V. *Tetrahedron Lett.* **2003**, *44*, 2083–2086.
18. Aamouche, A.; Devlin, F. J.; Stephens, P. J. *J. Am. Chem. Soc.* **2000**, *122*, 2346–2354.
19. Wilcox, C. S. *Tetrahedron Lett.* **2005**, *26*, 5749–5752.
20. Bailly, Ch.; Laine, W.; Demeunynck, M.; Lhomme, J. *Biochem. Biophys. Res. Commun.* **2000**, *273*, 681–685.

21. Baldeyrou, B.; Tardy, Ch.; Bailly, Ch.; Colson, P.; Houssier, C.; Charmantray, F.; Demeunynck, M. *Eur. J. Med. Chem.* **2002**, *37*, 315–322.
22. Tatibouët, A.; Demeunynck, M.; Andraud, Ch.; Collet, A.; Lhomme, J. *Chem. Commun.* **1999**, 161–162.
23. Nezu, T.; Ikeda, S. *Bull. Chem. Soc. Jpn.* **1993**, *66*, 18–24.
24. Ohyama, T.; Mita, H.; Yamamoto, Y. *Biophys. Chem.* **2005**, *113*, 53–59.
25. Synytsya, A.; Král, V.; Blechová, M.; Volka, K. *J. Photochem. Photobiol. B: Biol.* **2004**, *74*, 73–84.
26. Mudasir; Yoshioka, N.; Inoue, H. *J. Inorg. Biochem.* **1999**, *77*, 239–247.
27. Gawronski, J. K.; Polonski, T.; Lightner, D. A. *Tetrahedron* **1990**, *46*, 8053–8066.
28. Lightner, D. A.; An, J. *Tetrahedron* **1987**, *43*, 4287–4296.